International Journal of Rock Mechanics & Mining Sciences 78 (2015) 79–90

Contents lists available at ScienceDirect

International Journal of Rock Mechanics & Mining Sciences

journal homepage: www.elsevier.com/locate/ijrmms

Modelling 3D jointed rock masses using a lattice spring model

Gao-Feng Zhao [a,b,*]

[a] State Key Laboratory of Hydraulic Engineering Simulation and Safety, School of Civil Engineering, Tianjin University, Tianjin 300072, China
[b] Centre for Infrastructure Engineering and Safety, School of Civil and Environmental Engineering, The University of New South Wales, Sydney, NSW 2052, Australia

ARTICLE INFO

Article history:
Received 30 July 2014
Received in revised form
22 April 2015
Accepted 29 May 2015

Keywords:
Distinct lattice spring model
Jointed rock masses
Stability analysis
Failure

ABSTRACT

This study further develops the distinct lattice spring model (DLSM) to model jointed rock masses as a group of particles linked with spring bonds. This unified description of jointed rock masses is realised through the introduction of continuum- and discontinuum-based spring bonds into the DLSM. The joints are geometrically inputted as a group of triangles to aid in the generation of discontinuum-based spring bonds that are formed from a cutting operation between triangles and initial continuum-based spring bonds. A simple elasto-brittle model and Mohr–Coulomb constitutive model are introduced for the continuum- and discontinuum-based spring bonds to describe the mechanical responses of jointed rock masses. With these developments, the DLSM's ability to model jointed rock masses is demonstrated through numerical examples.

© 2015 Elsevier Ltd. All rights reserved.

1. Introduction

Modelling the mechanical behaviour of jointed rock masses is one of the most challenging tasks in rock engineering. Such modelling is directly related to the design and stability analysis of rock engineering structures that are built in or on jointed rock. Many numerical methods have been developed or further developed to address this problem, including the finite element method (FEM),[1] eXtended FEM (XFEM),[2] discrete element method (DEM),[3] discontinuous deformation analysis (DDA),[4] element-free Galerkin method (EFG),[5] natural element method,[6] smoothed particle hydrodynamics (SPH),[7] and boundary element method (BEM)[8]. In fact, the numerical methods used in rock engineering have been categorised into continuum-based and discontinuum-based methods according to their ability to solve jointed rock mass problems.[9] Continuum-based methods (e.g., the FEM and BEM) can model the macroscopic behaviour of jointed rock masses by implementing the corresponding macroscopic constitutive models, such as the damage-based model[10] and the Cosserat elasto-plastic model.[11] The main difficulty encountered with continuum-based approaches is the identification of suitable mechanical parameters for the jointed rock masses. Moreover, these approaches are not applicable when the rock cannot be homogenised, as in the case of a rock slope with only a few intersected joints. Researchers have proposed many solutions to explicitly model jointed rock masses, and some methods have been specifically developed for jointed rock masses, such as the DEM[3] and the DDA.[4] However, many studies have been also performed to enhance the ability of existing methods to model jointed rock masses as well (e.g., Refs. [1,2,5–8]).

Geometric and mechanical representations of joints are required to enhance a numerical method so that it can handle jointed rock masses. According to a review of the literature, there are three approaches to creating geometric representations: (a) describe the joint as a thin layer with weak material properties [12]; (b) model the joint as an interface or a contact[1,3,4]; and (c) represent the joints in an implicit manner.[2,13] The first approach is straightforward and free of additional modification to the classical FEM. An application of this approach can be found in the work of Tang and his co-workers.[12,14] The shortcomings of this approach include the high computational cost and the fact that the mechanical behaviour of joints cannot be precisely modelled. The second approach is the classical technique adopted in many numerical methods. The most notable contributions to this approach are the work performed by Goodman et al.[1] and the 3D joint elements developed by Beer[15] for FEM. However, issues arise when there are many joints. To tackle this problem, Shi developed a new numerical method for jointed rock, known as DDA.[4] The advantage of DDA is that the mechanical behaviour of joints can be precisely modelled. However, its implementation is complex, especially in 3D cases. In fact, the main shortcoming of

* Corresponding author at: The University of New South Wales, School of Civil and Environmental Engineering, Centre for Infrastructure Engineering and Safety, Sydney, NSW 2052, Australia. Fax: +61 2 9385 5022.
E-mail address: gzhaomech@outlook.com

http://dx.doi.org/10.1016/j.ijrmms.2015.05.011
1365-1609/© 2015 Elsevier Ltd. All rights reserved.

the second approach is the difficulty of preparing a computational model, particularly for 3D cases. This difficulty can be overcome by using the third approach, in which joints are represented implicitly. A notable example is the XFEM,[2] in which the level set method[16] has been adapted to model joints. Another example is the smooth joint contact model developed by Itasca Inc.[13] for their particle-based DEM code, in which the joints are inputted as being independent from the computational model and are used only for the purpose of modifying the particle contact direction and contact properties.[13] Mechanical representation is another important issue for joints. Numerous approaches have been developed, such as the spring/penalty method,[2,3] the penalty function method,[17] the augmented Lagrangian method,[18] and the complementary theory.[19] Among these methods, the spring/penalty method is the most popular due to its ease of implementation and thoroughly understood and measurable parameters (e.g., the normal and shear joint stiffness, cohesion, friction angle, and tension strength, all of which can be determined from classical rock experiments).

In this work, the distinct lattice spring model (DLSM)[20] is further developed for jointed rock masses. The particle based numerical models can be subdivided into continuum-based models (e.g. EFG and SPH) and discontinuum-based models (e.g. DEM and DLSM). The continuum-based model adopts the top-to-bottom methodology, whereas, the discontinuum- based one uses the bottom-to-top methodology. This methodological difference results in equivalent components of these models might have different meanings. For example, as the requirement of convergence, influence of particle distribution and particle size of EFG and SPH is supposed to be small enough and is treated as a numerical error. However, for most cases, this influence is the target of discontinuum-based modelling. Overall, continuum-based models tackle mechanical problem by solving partial differential equations, whereas, discontinuum-based models attempt to rebuild a virtual approximate system physically. Discontinuum-based models are believed to have the advantage over continuum-based counterparts on simulation of nonlinear problems involving dynamic topological change and discrete behaviour, e.g., dynamic fracturing and fragmentation. As a newly developed discontinuum-based model, compared with the DEM, advantages of the DLSM are: i) it can directly use macroscopic elastic parameters without any requirement for calibration; and ii) it uses only half of the Degree of Freedoms (DOFs) compared with the DEM. The DLSM was originally developed to model the dynamic failure of intact rock,[20] and a detailed overview of the DLSM and its development can be found in Ref. [21]. The thin layer approach had been adopted in the DLSM to represent discontinuity in Ref. 32. A considerable amount of particles were utilised to represent a single joint (three to four layers of particles). In this work, jointed rock masses are conceptually discretised into a group of particles linked through continuum- and discontinuum-based spring bonds. An implicit representation of the joints is adopted in which joints are geometrically represented through a group of triangles to assist with the generation of discontinuum-based spring bonds. In this new approach, there is only single layer of discontinuum-based springs for each joint, therefore, it is much more computationally efficiency than the thin layer approach adopted in Ref. 32. Finally, constitutive models of the continuum- and discontinuum-based spring bonds are introduced to represent the mechanical behaviour of jointed rock masses (for which the spring/penalty method is adopted). Using these techniques the DLSM is successfully extended to solve problems involving jointed rock masses. The implementation is verified by a number of examples comparing both the analytical and experimental results.

2. Model

This section focuses on the new extensions created for the DLSM to model jointed rock masses. A brief introduction of the DLSM is provided in this section. More details can be found in the work of Zhao et al.[20]

In the DLSM, rock is represented as an assemblage of mass particles with different sizes. As shown in Fig. 1, whenever the gap between two particles is smaller than a given threshold value, a bond between the two particles will be formed. Fig. 1b shows the calculation cycle of the DLSM.[20] Given the particle displacements (either prescribed initially or obtained from the previous time step), broken bonds and new contacts are detected. For each particle, the list of neighbouring particles is updated. Then, contact and spring forces between particles are calculated according to the prescribed constitutive model (the force–displacement relation). The particle velocity is calculated as

$$\dot{u}_{i,t+\Delta t/2} = \dot{u}_{i,t-\Delta t/2} + \frac{\sum F_{j,t}}{m_p}\Delta t \tag{1}$$

where $\dot{u}_{i,t+\Delta t/2}$ is the particle velocity at $t + \Delta t/2$, $\dot{u}_{i,t-\Delta t/2}$ the particle velocity at $t - \Delta t/2$, m_p the particle mass, $\sum F_{j,t}$ the sum of forces acting on the particle i including applied external forces, and Δt the time step. New displacement of the particle is advanced as

$$u_{i,t+\Delta t} = u_{i,t} + \dot{u}_{i,t+\Delta t/2}\Delta t \tag{2}$$

in which $u_{i,t+\Delta t}$ is the displacement at $t + \Delta t$, $u_{i,t}$ the displacement at t.

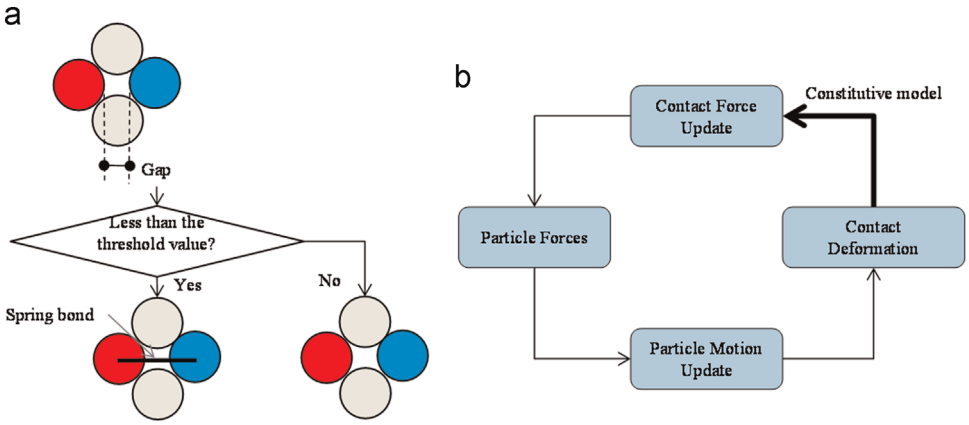

Fig. 1. Lattice generation and calculation cycle of the DLSM.

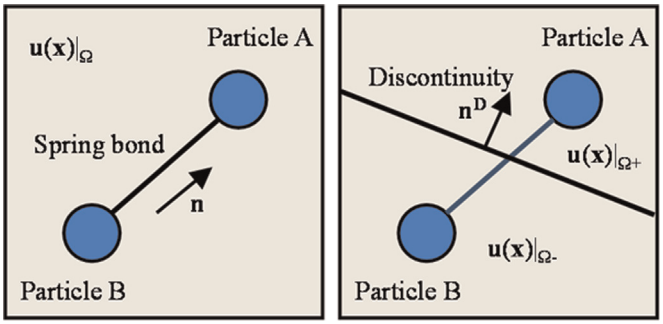

Fig. 2. Two types of spring bonds developed for the DLSM to represent jointed rock masses.

In the DLSM, different threshold values can produce different lattice structures. Influence of different lattice structures on the modelling results has been studied in.[20] It was found that the lattice model with cubic II, bcc I, bcc II and random structure can provide a good agreement with the FEM solution.[20] For cubic II lattice used in this paper, the threshold value is taken as half of the particle size.

2.1. Continuum- and discontinuum-based spring bonds

The basic concept of the DLSM is to discretise rock into particles linked with spring bonds. When adopting this concept for jointed rock masses, as shown in Fig. 2, there will be two types of spring bonds, continuum-based and discontinuum-based spring bonds. The continuum-based spring is used to represent the mechanical behaviour of a unit of the rock block. Its represented unit Ω is continuous, the deformation of which is described by a displacement function as $\mathrm{u(x)}|_{\Omega}$. The 1st order displacement function was adopted in the DSLM.[20] Assume the positions of the two particles are x_A and x_B, and the normal direction of the spring bond is then

$$\mathrm{n}=\frac{\mathrm{x}_B-\mathrm{x}_A}{l} \tag{3}$$

where l is the length of the spring bond. If the displacements of two particles are u_A and u_B, the normal deformation of the spring bond can be calculated as

$$\mathrm{u}^n=\left((\mathrm{u}_B-\mathrm{u}_A)\cdot\mathrm{n}\right)\mathrm{n} \tag{4}$$

To remove rigid body rotation in the DLSM,[20] the shear deformation is obtained as

$$\mathrm{u}^s=[\varepsilon]\cdot\mathrm{n}l-(([\varepsilon]\cdot\mathrm{n}l)\cdot\mathrm{n})\mathrm{n} \tag{5}$$

where $[\varepsilon]$ is the strain tensor of the represented unit (particle cluster), which is determined by the displacement function $\mathrm{u(x)}|_{\Omega}$ through the least-squares method. Eq. (5) is to calculate the multi-body shear deformation. The purpose of using the local strain is to get rid of the influence of the rigid body rotation, which is important to solve the Poisson's limitation in the classical Lattice Spring Model (LSM). Details on the derivation of Eq. (5) are explained in Appendix A of Ref. 20 The interaction force between particles A and B is given as

$$\mathrm{F}_{AB}=k_n\mathrm{u}^n+k_s\mathrm{u}^s \tag{6}$$

where F_{AB} is the interaction force from particle B to particle A due to spring deformation, and k_n and k_s are the normal and shear spring stiffness respectively.

The discontinuum-based spring bond represents the mechanical behaviour of a unit containing a joint. Geometrically, the unit is made up of two parts represented by Ω^+ and Ω^-. The corresponding displacement functions for these two parts are written as $\mathrm{u(x)}|_{\Omega^+}$ and $\mathrm{u(x)}|_{\Omega^-}$. There is only one particle in each portion (Ω^+ and Ω^-) of the discontinuum-based cube (see Fig. 2b). Therefore, the zero order displacement function is able to represent the deformation state of these two portions as

$$\mathrm{u(x)}|_{\Omega^-}=\mathrm{u}_A \tag{7}$$

$$\mathrm{u(x)}|_{\Omega^+}=\mathrm{u}_B \tag{8}$$

The deformation between the two particles is concentrated on the joint, and the deformation along the joint's normal direction is expressed as

$$\mathrm{u}_D^n=\left((\mathrm{u}_B-\mathrm{u}_A)\cdot\mathrm{n}^D\right)\mathrm{n}^D \tag{9}$$

where n^D is the normal direction of the discontinuity (see Fig. 2b).

Within a discontinuum-based cube (see Fig. 2b), interaction between two particles is in a two-body state, therefore, the shear deformation is directly calculated from particle displacements. The shear deformation of the joint is calculated as

$$\mathrm{u}_D^s=(\mathrm{u}_B-\mathrm{u}_A)-\left((\mathrm{u}_B-\mathrm{u}_A)\cdot\mathrm{n}^D\right)\mathrm{n}^D \tag{10}$$

The interaction force between particles A and B for the discontinuum-based spring bond is

$$\mathrm{F}_{AB}^D=k_n^D\mathrm{u}_D^n+k_s^D\mathrm{u}_D^s \tag{11}$$

where k_s^D and k_n^D are the normal and shear spring stiffness for the discontinuum-based spring bond respectively.

It should be mentioned that the discontinuum-based spring bond takes the same form as the typical point-to-point contact developed for the FEM. The discontinuum-based spring bond has also been unsuccessfully adopted in the LSM to model continuum problems.[22] To tackle this problem, the multi-body shear spring has been developed and is a main contribution and distinct feature of the DLSM.[20] Interestingly, however, the discontinuum-based spring bond (the previously unsuccessful solution for continuum) is now integrated into the DLSM for jointed rock masses (discontinuum). This adoption could provide insight on the discontinuous nature of the jointed rock from the multi-body interaction and rigid body rotation viewpoints.

2.2. Representation of joints

Joints can be highly irregular surfaces. A group of triangles is a direct and effective solution for representing these surfaces. In the DLSM, as shown in Fig. 3, different joints are described using a group of triangles. Two set of joints may have intersections, but the intersections do not have to be modelled explicitly (see Fig. 3d). This feature simplifies the requirements of model preparation. For example, a simple geometric cutting operation and triangular mesh generation are required to prepare the data for typical jointed rock masses. The triangles for the joints shown in Fig. 3a and b are generated from a cutting operation performed between a cube and a plane. The first step is to obtain the intersection points between the plane and the cube. Next, triangles are formed using the Delaunay triangulation on these intersection points.[23] Jointed rock masses are then geometrically represented by joints and particles (see Fig. 3). Their mechanical responses are modelled by the continuum- and discontinuum-based spring bonds. Continuum-based spring bonds are formed between two particles when the gap is smaller than a given threshold value,[20] while discontinuum-based spring bonds are generated from a cutting operation between the initial continuum-based spring bonds and the triangles. If a continuum-based spring bond is cut by a triangle, then it is turned into a discontinuum-based spring

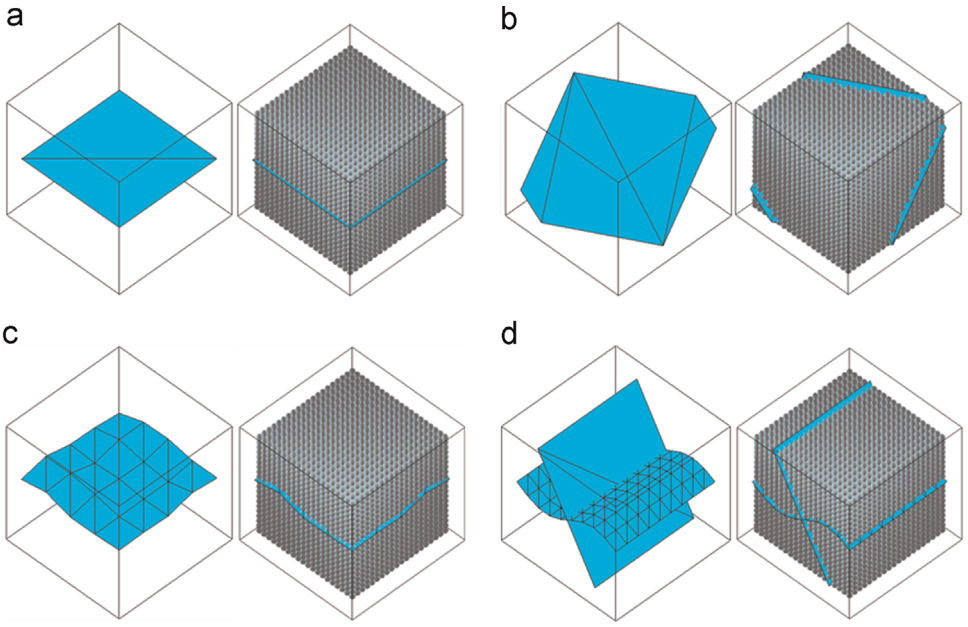

Fig. 3. Geometric representations of joints using a group of triangles in the DLSM.

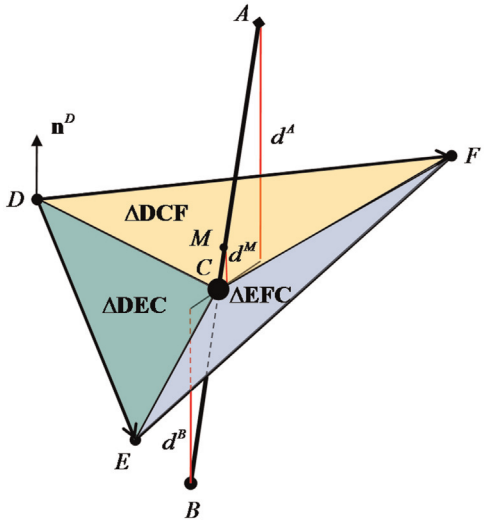

Fig. 4. Cutting operation between a continuum-based spring bond and a triangle.

bond. As shown in Fig. 4, the continuum-based spring bond is represented by $\overrightarrow{AB}$ and the triangle is represented by ΔDEF. The plane containing the triangle is presented with a vertex (e.g., **D**) and a vector of the plane's normal direction, which is written as

$$\mathrm{n}^D = \frac{\overrightarrow{\mathrm{DE}} \times \overrightarrow{\mathrm{DF}}}{\|\overrightarrow{\mathrm{DE}} \times \overrightarrow{\mathrm{DF}}\|} \tag{12}$$

The sign distances from the two vertices of the continuum-based bond to the plane $(\mathrm{D},\mathrm{n}^D)$ are then calculated as

$$d^A = \mathrm{n}^D \times \overrightarrow{\mathrm{DA}} \tag{13}$$

$$d^B = \mathrm{n}^D \times \overrightarrow{\mathrm{DB}} \tag{14}$$

The cutting algorithm is described as follows. It should be mentioned that the following instructions must be performed in a sequential manner. If $d^A=0$ and $d^B=0$, the spring bond is on the plane, and the calculation is concluded. If $d^A \cdot d^B > 0$, the spring bond is outside of the plane and the calculation is concluded. If $d^A \cdot d^B = 0$, the distance of the bond's middle point M to the plane is needed.

$$d^M = \mathrm{n}^D \times \overrightarrow{\mathrm{DM}} \tag{15}$$

The exit calculation condition is $d^m < 0$; otherwise, the calculation is continued. This additional judgment is necessary to prevent a triangle from cutting particle on it twice. If $d^A \cdot d^B < 0$, then the calculation is continued.

After the first round of judgment, the cross point (**C**) of the bond and the plane is calculated for further analysis. As shown in Fig. 4, the following relationship exists:

$$\frac{\|\mathrm{AC}\|}{\|\mathrm{AB}\|} = \frac{d^A}{d^A - d^B} \tag{16}$$

The cross point can be obtained as

$$\mathrm{C} = \mathrm{A} + \overrightarrow{\mathrm{AB}} \frac{d^A}{d^A - d^B} \tag{17}$$

The areas of triangles ΔDEF, ΔDEC, ΔEFC, and ΔFDC are then calculated as

$$S^{DEF} = \frac{\|\overrightarrow{\mathrm{DE}} \times \overrightarrow{\mathrm{DF}}\|}{2} \tag{18}$$

$$S^{DEC} = \frac{\|\overrightarrow{\mathrm{DE}} \times \overrightarrow{\mathrm{DC}}\|}{2} \tag{19}$$

$$S^{EFC} = \frac{\|\overrightarrow{\mathrm{EF}} \times \overrightarrow{\mathrm{EC}}\|}{2} \tag{20}$$

$$S^{FDC} = \frac{\|\overrightarrow{\mathrm{FD}} \times \overrightarrow{\mathrm{FC}}\|}{2} \tag{21}$$

The condition for the cross point to lie outside the triangle is

$$S^{DEC} + S^{EFC} + S^{FDC} > S^{DEF} \tag{22}$$

The spring bond is marked as a discontinuum-based spring bond when the cross point is not outside of the triangle. Eq. (22) can also be represented as the condition of the cross point in the

triangle, while the current form is more robust for computer implementation. The cutting operation is repeated until all of the continuum-based spring bonds and joints have been scanned.

The cutting algorithm described here can guarantee that there is one and only one linked triangle for each discontinuum-based spring bond. This guarantee is from the strict requirement on the sequential operation. When a continuum-based spring bond is cut by a triangle, it will be kicked out from the group of continuum-based spring bonds since it is no longer a continuum-base spring bond. It is a simplified coalescence treatment for cases when a continuum-based spring bond might be cut by multiple triangles. The cutting algorithm also records the number of continuum-based spring bonds cut by each triangle n^{TC}. The representative area of a discontinuum-based spring bond is calculated as

$$A^D = \frac{S^{DEF}}{n^{TC}} \tag{23}$$

where S^{DEF} is the area of the linked triangle and n^{TC} is the total number of continuum-based spring bonds cut by the triangle.

Size of the triangle cannot influence simulation results apparently until the triangle is so small that it cannot cut any spring bond. In actual modelling, the triangle mesh is generated from a triangulation of vertexes of the joint. The purpose of using a triangle mesh is to simplify the geometric representation. It should be mentioned that polygons and implicit surface equations can be employed in the DLSM to represent joints as well.

After the cutting operation, the joints are represented by a group of discontinuum-based spring bonds. This approach is similar to the smooth joint model developed by Itasca Inc.[13] The main function of the smooth joint is to change the direction of contact between two cut particles. Additional microparameters for this contact are introduced and further calibration is required.[13] The main improvements of the techniques developed in this work provide to the DLSM are (a) the geometrical representation of joints by a group of triangles and (b) the calculation of a representative area of a discontinuum-based spring bond that can be used to directly calculate the micromechanical parameters of the discontinuum bonds based the corresponding macroscopic parameters (see the following section).

2.3. Constitutive model

The rock block in the DLSM is modelled by a group of continuum-based spring bonds. A simple elasto-brittle constitutive model is adopted for this task (Fig. 5). The force–displacement relationships of the normal and shear springs are given as

$$\mathrm{F}^n = \begin{cases} k_n \cdot \mathrm{u}^n & , \text{ else} \\ 0 & , \ \mathrm{u}^n \cdot \mathrm{n} \geq u_n^* \end{cases} \tag{24}$$

$$\mathrm{F}^s = \begin{cases} k_s \cdot \mathrm{u}^s & , \ \|\mathrm{u}^s\| < u_s^* \text{ and } \mathrm{u}^n \cdot \mathrm{n} < u_n^* \\ 0 & , \text{ else} \end{cases} \tag{25}$$

where k_n and k_s are the normal and shear spring stiffness, respectively, u^n and u^s are obtained from Eqs. (4) and (5), respectively, and u_n^* and are the threshold values of limit deformation for the normal and shear springs, respectively. When failure occurs, u_n^* is set to zero. The normal and shear spring stiffness are calculated using the following equations[20]:

$$k_n = \frac{3E}{2\alpha^{3D}(1-2\nu)} \tag{26}$$

$$k_s = \frac{3(1-4\nu)E}{2\alpha^{3D}(1+\nu)(1-2\nu)} \tag{27}$$

where E is the Young's modulus and ν is the Poisson's ratio. a^{3D} is a microstructure geometry coefficient of the lattice model, which is given as[20]

$$a^{3D} = \frac{\sum l_i^2}{V} \tag{28}$$

where l_i is the original length of the ith spring bond and V is the volume of the represented geometry model. Details on the derivation and verification of Eqs. (26)–(28) can be found in Ref. [20]

The constitutive model of a discontinuum-based spring bond is shown in Fig. 6. The force and displacement relationships are written as

$$\mathrm{F}^n = \begin{cases} k_n^D \cdot \mathrm{u}_D^n & , \ k_n^D(\mathrm{u}^n \cdot \mathrm{n}) < \sigma_t^J A^D \\ 0 & , \text{ else} \end{cases} \tag{29}$$

$$\mathrm{F}^s = \begin{cases} k_s^D \cdot \mathrm{u}_D^s & , \ k_s^D \|\mathrm{u}_D^s\| < c^J A^D + (\mathrm{F}_n \cdot \mathrm{n}) \cdot \tan \varphi^J \\ (\mathrm{F}_n \cdot \mathrm{n}) \cdot \tan \varphi^J \mathrm{u}_D^s / \|\mathrm{u}_D^s\| & , \text{ else} \end{cases} \tag{30}$$

where k_s^D and k_n^D are the normal and shear spring stiffness, respectively, u_D^n and u_D^s are the spring deformations obtained from

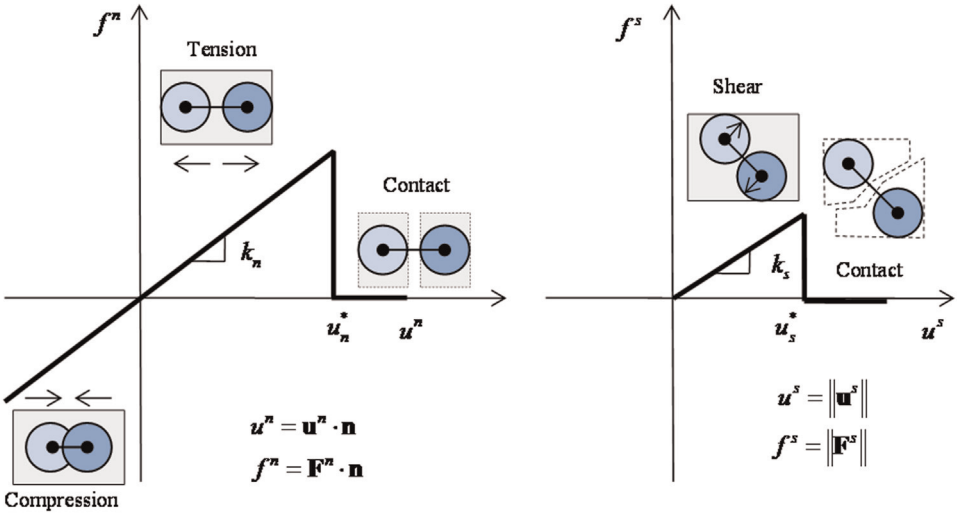

Fig. 5. Elasto-brittle constitutive model for the continuum-based spring bond.

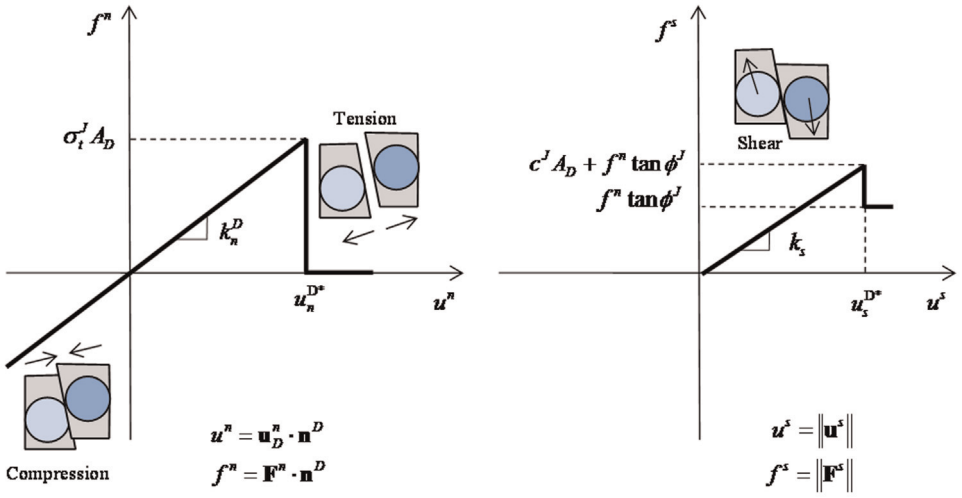

Fig. 6. Mohr–Coulomb constitutive model for the discontinuum-based spring bond.

Eqs. (9) and (10), respectively, σ_t^J is the tensile strength of the joint, c^J is its cohesion, ϕ_t^J is its friction angle, and A^D is the representative area of the discontinuum-based spring bond. When a discontinuum-based spring bond is broken, the tensile strength and cohesion are both reduced to zero which is a contact treatment under small deformation. The shear and normal spring stiffness of a discontinuum-based spring bond are calculated as

$$k_n^D = k_n^J A^D \tag{31}$$

$$k_s^D = k_s^J A^D \tag{32}$$

where k_n^J and k_s^J are the normal and shear stiffness of the joint, respectively. It should be mentioned that the constitutive model represented by Eqs. (29) and (30) is a simplified Coulomb model which cannot consider the unloading and reloading behaviour of rock joints. More advanced models can be implemented into the DLSM as well. For example, an Unloading–Reloading–Dilation (URD) constitutive model for the DLSM was presented as follows.

The Unloading–Reloading–Dilation (URD) constitutive model is shown in Fig. 7. The red line in Fig. 7a represents the simplified Coulomb criterion based model. Additional loop is added to reflect the unloading and reloading behaviour. The dilation model is illustrated in Fig. 7b. To consider the unloading–reloading behaviour, the shear deformation is decomposed as:

$$\mathrm{u}_D^s = \mathrm{u}_D^{se} + \mathrm{u}_D^{sp} \tag{33}$$

where u_D^s is the total shear deformation, u_D^{se} is the elastic deformation part and u_D^{sp} is the plastic/sliding component. The shearing force is only related to the elastic part

$$\mathrm{F}_D^s = \mathrm{u}_D^{se} k_s^D \tag{34}$$

where k_s^D is the stiffness of the discontinuum-based shear spring. To consider dilation of the discontinuum-based shear spring, Eq. (29) is further modified as:

$$\mathrm{F}_D^n = \begin{cases} k_n^D \cdot \left(\mathrm{u}_D^n + u_{dl}^n \mathrm{n}^D\right) & , \; k_n^D \left(\mathrm{u}_D^n \cdot \mathrm{n}^D + u_{dl}^n\right) < \sigma_t^J A^D \\ 0 & , \; \text{else} \end{cases} \tag{35}$$

where u_{dl}^n is the dilational component of the normal deformation. It is calculated as

$$u_{dl}^n = \begin{cases} 0 & , \; \|\mathrm{u}_D^s\| < u_{dl}^{res} \\ \tan\psi\left(\|\mathrm{u}_D^s\| - u_{dl}^{res}\right) & , \; \text{else} \\ \tan\psi\left(u_{dl}^{cs} - u_{dl}^{res}\right) & , \; \|\mathrm{u}_D^s\| > u_{dl}^{cs} \end{cases} \tag{36}$$

in which u_{dl}^{cs} is the limiting value for further dilation. The u_{dl}^{res} is the initial condition of dilating which is given as

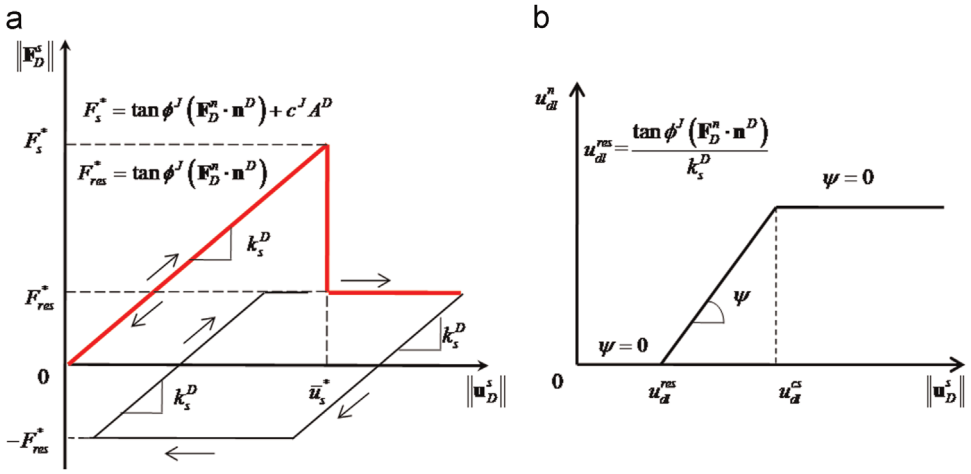

Fig. 7. Unloading–Reloading–Dilation (URD) constitutive model for the discontinuum-based shear spring. (For interpretation of the references to colour in this figure legend, the reader is referred to the web version of this article.)

$$u_{dl}^{res} = \frac{\tan\ \phi^J\left(\mathrm{F}_D^n \cdot \mathrm{n}^D\right)}{k_s^D} \tag{37}$$

The URD constitutive model represented by Eqs. (33)–(37) is a typical nonlinear model. To implement it into the DLSM, these equations are further discretized into the time domain as

$$\mathrm{F}_{D,t}^n = k_n^D\left(\mathrm{u}_{D,t}^n + u_{dl,t-\Delta t}^n \mathrm{n}^D\right) \tag{38}$$

where $\mathrm{F}_{D,t}^n$ is the normal force at current time step, $\mathrm{u}_{D,t}^n$ is the normal deformation at current time step, and $u_{dl,t-\Delta t}^n$ is the dilational normal deformation of the previous time step.

The trial shearing force at current time step is calculated as

$$\bar{\mathrm{F}}_{D,t}^s = k_s^D\left(\mathrm{u}_{D,t-\Delta t}^{se} - \mathrm{u}_{D,t-\Delta t}^s + \mathrm{u}_{D,t}^s\right) \tag{39}$$

in which $\mathrm{u}_{D,t-\Delta t}^{se}$ is the elastic shear deformation of the previous time step, $\mathrm{u}_{D,t-\Delta t}^s$ is the total deformation of the previous time step, and $\mathrm{u}_{D,t}^s$ is the current total shear deformation.

The initial dilating deformation at current time step is given as

$$u_{dl,t}^{res} = \frac{\tan\ \phi^J\left(\mathrm{F}_{D,t}^n \cdot \mathrm{n}^D\right)}{k_s^D} \tag{40}$$

The dilational normal deformation at current time step is obtained as

$$u_{dl,t}^n = \begin{cases} 0 & ,\ \|\mathrm{u}_{D,t}^s\| < u_{dl,t}^{res} \\ \tan\ \psi\left(\|\mathrm{u}_{D,t}^s\| - u_{dl,t}^{res}\right) & ,\ \text{else} \\ \tan\ \psi\left(u_{dl}^{cs} - u_{dl,t}^{res}\right) & ,\ \|\mathrm{u}_{D,t}^s\| > u_{dl}^{cs} \end{cases} \tag{41}$$

The shear force at current time step is calculated as

$$\mathrm{F}_{D,t}^s = \begin{cases} \bar{\mathrm{F}}_{D,t}^s & ,\ \|\bar{\mathrm{F}}_{D,t}^s\| <= \tan\ \phi^J \|\mathrm{F}_{D,t}^n\| \\ \bar{\mathrm{F}}_{D,t}^s \dfrac{\tan\ \phi^J \|\mathrm{F}_{D,t}^n\|}{\|\bar{\mathrm{F}}_{D,t}^s\|} & ,\ \text{else} \end{cases} \tag{42}$$

The elastic shear deformation at current time step is

$$\mathrm{u}_{D,t}^{se} = \frac{\mathrm{F}_{D,t}^s}{k_s^D} \tag{43}$$

The URD constitutive model was used to solve all the examples in the paper (dilation angle=0°). It was found that the same results were obtained compared with these by using the simplified Coulomb model. Due to advantages of the simplified Coulomb model on memory and computational time saving, it is still recommended to be used for monotonic loading dominated condition. Different joint models can be implemented into the DLSM. For intact rocks, different cohesive models can also be implemented.[31] However, as a newly developed model, more sophisticated constitutive models for DLSM are still badly needed. For example, joint persistence is a parameter dominating the actual rock masses strength. For the DLSM, there are two possible solutions to consider joint persistence. The first one is to directly rebuild the rock bridge configuration. However, directly mapping these joints into actual models is impossible on a practical basis due to the demanding computational requirement. A feasible solution would be implementation of a joint constitutive model to incorporate the joint persistence, which will be a future research direction of the DLSM.

Using the geometrical representation method, the cutting algorithm, and the constitutive models, the DLSM can then solve jointed rock masses. Compared with the existing numerical methods for solving jointed rock masses, the advantages of the DLSM are (a) its straightforward implementation and (b) its lack of micro-parameter calibration provided by the original DLSM compared with the particle-based DEM. The main concern lies in whether this simple implementation can solve jointed rock mass problems with reasonably accurate results, a question addressed in the following section.

3. Numerical examples

In this section, numerical examples of typical problems involving jointed rock masses are solved using the improved DLSM.

3.1. Uniaxial compression of a block with a single joint

This problem is illustrated in Fig. 8a. A pressure p is applied on the top surface of a block with a joint, while the bottom is fixed. The analytical solution of the top surface's deformation from adding the deformation of the intact block and deformation of the joint as

$$u = \frac{L^* p}{E} + \frac{p}{k_n} \tag{44}$$

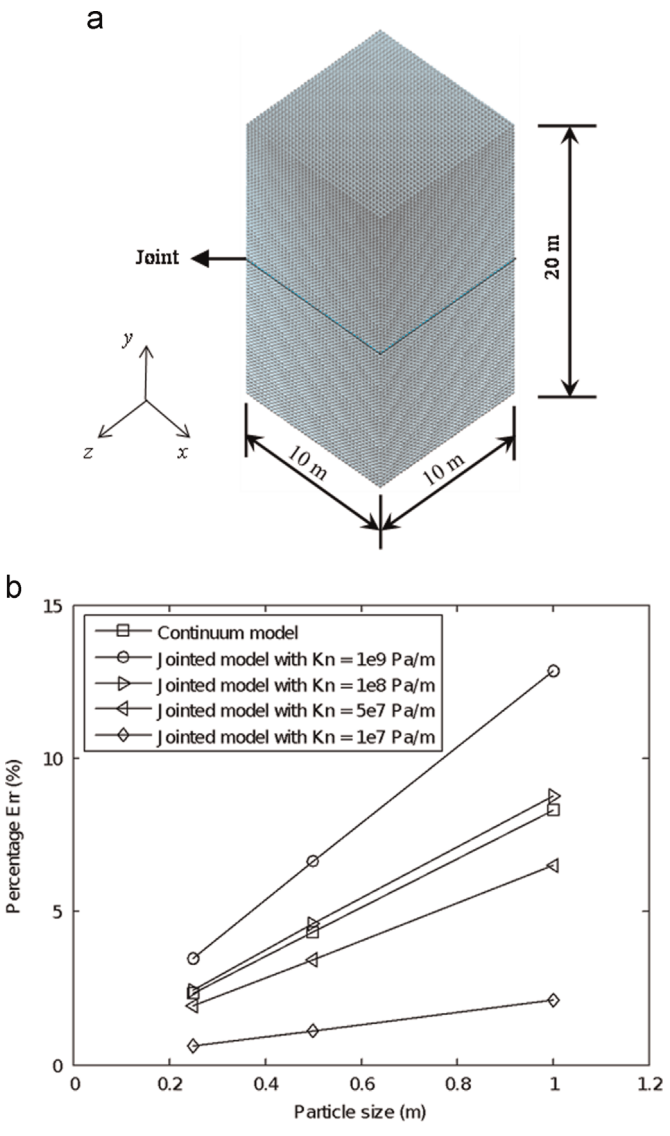

Fig. 8. DLSM simulation of the uniaxial compressive test performed on a block with a joint.

where u is the top surface's displacement, L^* is the effective length of the block, $L^* = L - d$ (where L is the length of the block and d is the particle size), p is the applied pressure, E is the elastic modulus, and k_n is the normal stiffness of the joint.

A computation model created in the DLSM for this problem is shown in Fig. 8a. The dimension of the block is 10 m × 20 m × 10 m, the applied pressure is 1 MPa, the elastic modulus is 1 GPa, Poisson's ratio is 0.2, and the density is 2450 kg/m^3, while the particle size d and joint normal stiffness k_n are varied as 10 MPa/m, 50 MPa/m,100 MPa/m and 1000 MPa/m. The ratio between joint's shear and normal stiffness is taken one. The results predicted by the DLSM are compared with the analytical solution (see Fig. 8b), indicating that the numerical results are in good agreement with the analytical results. The numerical error of the DLSM can be reduced by decreasing the particle size or joint stiffness. It is interesting to note that the DLSM can produce even more accurate results for a jointed block with low stiffness than for a continuum block because when the stiffness of the joint is small, the analytical solution (Eq. (44)) is controlled mainly by the joint's normal deformation. This result shows that the joint deformation modelled by the DLSM is accurate, and the example indicates that the DLSM is capable of correctly modelling the normal deformation of a joint. As mentioned in Section 1, influence of particle size in a discontinuum based model has a different meaning compared that in a continuum based model. In this paper, the numerical modelling is regarded as convergence when the error between analytical and numerical solutions are in a small range.

3.2. Sliding block

The previous example tests the ability of the DLSM to model the normal deformation of a joint. In this section, the shear deformation is tested, and the sliding box problem is an appropriate example for this purpose (see Fig. 9a). A block measuring 5 m × 5 m × 10 m is placed on a table measuring 5 m × 100 m × 100 m. The particle size of the block and table are both 1 m and the table's angle of incline is 45°. The material parameters of the box and table are an elastic modulus of 32 GPa, the Poisson's ratio of 0.25, and density of 2450 kg/m^3. The joint normal and shear stiffness are taken as 50 GPa/m. When subjected to gravity, the block will slide along the table surface. A joint is placed between the block and table to simulate a flat surface, and the analytical solution of the block's sliding distance[26] is given as

$$u = \frac{1}{2} g(\sin(\alpha) - \tan(\varphi)\cos(\alpha))t^2 \tag{45}$$

where g is gravity, α is the angle of incline (45° in this example), and t is the sliding time. The analytic solution and corresponding results predicted by the DLSM under different friction angles (10, 20, and 30) are shown in Fig. (9b), which indicates that the shear spring has been implemented correctly in the DLSM.

3.3. Wedge stability analysis

Hoek and Bray[24] provided an analytic solution for the factor of safety (FOS) in a 3D wedge problem, as shown in Fig. 10. The FOS is written as

$$\mathrm{FOS} = \frac{(F_A + F_B)\tan\ \varphi}{W\ \sin\ \psi} \tag{46}$$

where F_A and F_B are the reaction forces normal to planes A and B, respectively, φ is the friction angle of the planes, W is the wedge's weight, and ψ is the angle between the intersection line of planes A and B with the horizontal plane.

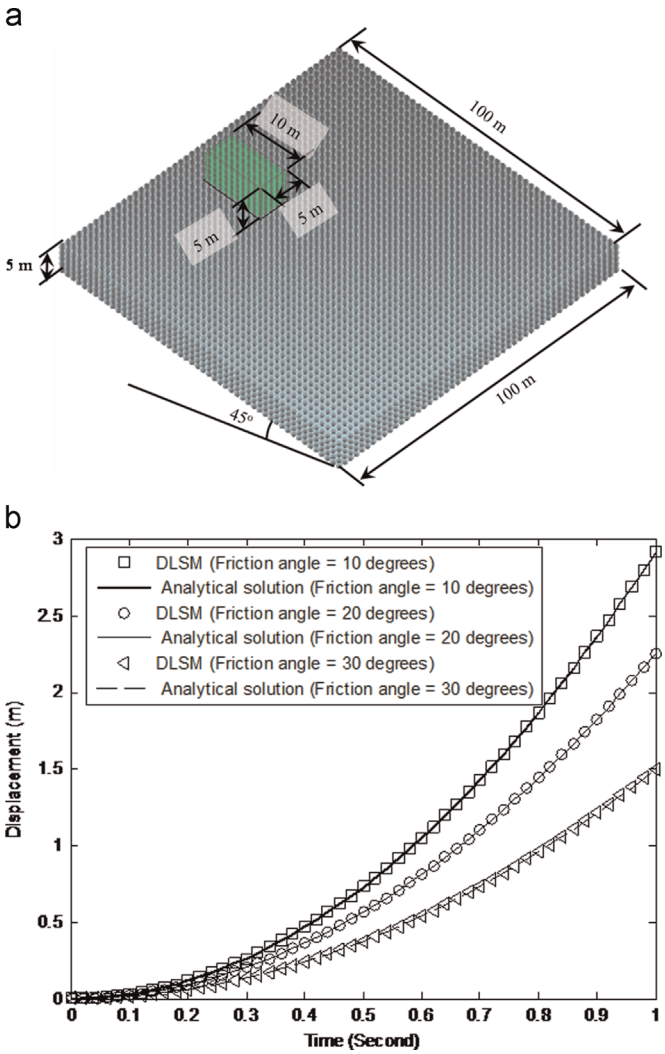

Fig. 9. DLSM simulation of a block sliding on an inclined table.

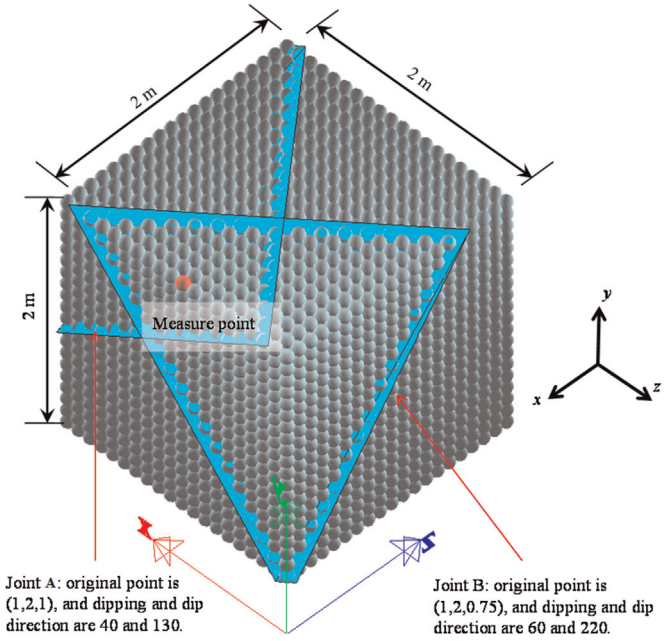

Fig. 10. 3D wedge model used for stability analysis in the DLSM.

The computational model for this problem in the DLSM is shown in Fig. 10. The dimension of the block is 2 m × 2 m × 2 m, the particle size is 0.1 m, and the model is made up of 8000 particles. Two sets of joints are inserted into the particle model to form the wedge shown in Fig. 10. The dip angle and dip direction of these two joints are (40, 130) and (60, 220), respectively (units in degrees), and the original points of these two joints are (0, 0, 1) and (0, −0.25, 1) (units in m). The material parameters rock block are: the Elastic modulus of 32 GPa, the Poisson's ratio of 0.25, and density of 2450 kg/m^3. The mechanical properties of the joints include shear and normal stiffnesses of 10 MPa/m, cohesion of 0 MPa, friction angle is varied to find the critical friction angle. In this work, the critical friction angle refers to the smallest stable friction angle. The analytical solution to the critical friction angle for this problem is 33.36°.[25]

The DLSM is used to calculate the critical friction angle. First, consolidation of the model under gravity is conducted. All the boundaries except the free surfaces of the 3D wedge are fixed with displacement in their normal direction, and the friction angle is set to a large value (89°). The solution results are used as the initial condition for further calculations using different friction angles. A detection point (0.95, 1.95, 0.05) (units in metres) is placed in the wedge to record the history of its vertical displacement. Due to rock blocks of this example are very stiff (close to rigid). The movement of the wedge is constrained by sliding planes A and B. More specifically, the movement in z direction is fixed and the ratio between x and y displacements is a constant value determined by normal directions of two sliding planes. Therefore, the displacement in y direction of a single point can be used to represent the movement of the whole wedge. Fig. 11 shows the displacement in y direction of the wedge predicted by the DLSM at friction angles varying from 30° to 40°. It can be seen that 34° is the critical friction angle. The curve of final displacement of the wedge at the end of simulation versus the friction angle confirms this angle (see Fig. 12).

The numerical error of the DLSM result is (34–33.36)/33.36 = 1.92%. This example indicates that the DLSM can predict a reasonable FOS for the 3D wedge problem, which is a typical 3D slope stability problem used to verify many numerical methods. [25,26] This example further proves that the representation of jointed rock masses using a group of particles linked through spring bonds in the DLSM is a feasible solution. The main purpose of this example is to test the ability of the enriched DLSM on solving stability problems of rock masses. In this example, the 8000-particles model produced a result of 1.82% error compared with the analytical solution. It was found that the same critical friction angle was obtained when a model of 15,625 particles was used. The results indicate that a relatively coarse particle model can be used in the DLSM.

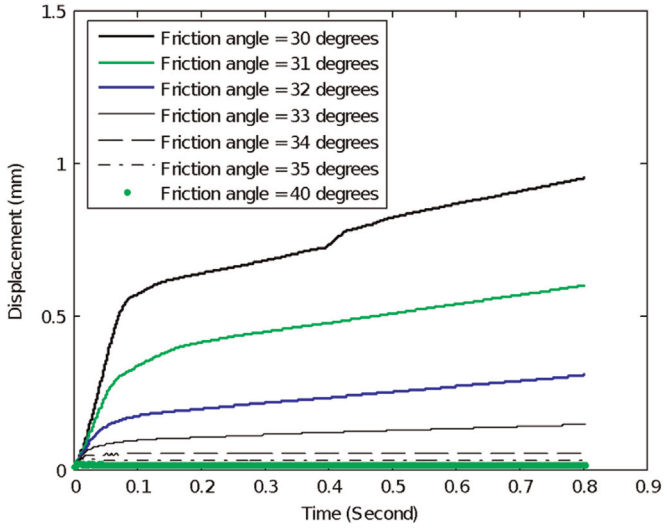

Fig. 11. Vertical displacement of the 3D wedge predicted by the DLSM using different friction angles.

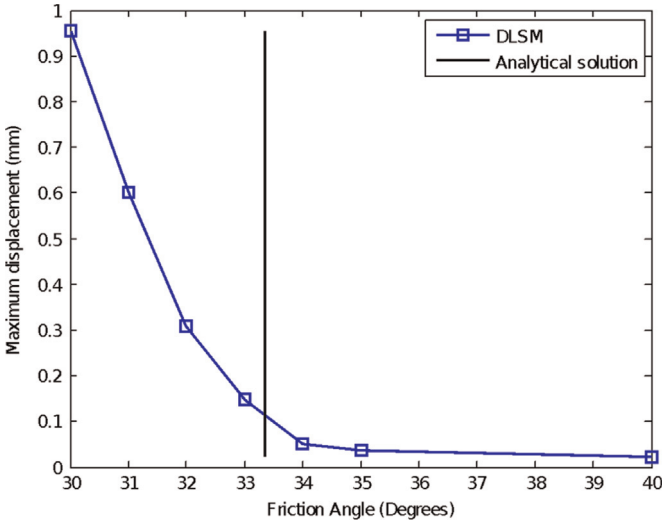

Fig. 12. Critical friction angle of the 3D wedge problem predicted by the DLSM.

3.4. Falling wedge analysis

In this section, the stability of a 3D rock wedge in the ceiling of an excavation is studied using the DLSM. This scenario is a classical problem in tunnelling engineering involving jointed rock masses. [25] The effect of the in-situ stresses and joint stiffness are important to this problem. The wedge is formed by three joints dipping at 60° and with dip directions of 30°, 150° and 270°, respectively (see Fig. 13a). The height of the wedge is 1 m, and the in-situ stress has two principal stresses parallel to the excavation roof (equal to −0.05 MPa). The vertical principal stress is zero. The analytical solution of this problem has been given by Goodman et al. (1982).[27] As shown in Fig. 13a, all the joints have the same dip angle, the initial stress in the plane parallel to the free face of the block is hydrostatic and all the joints have the same ratio between their normal and shear stiffnesses. For this specific case, the friction coefficient (equal to all joints) required for stability of the wedge without any support is expressed as[25]

$$\tan\ \varphi = \frac{W + \sigma_n \sum A_i \sin\ \alpha}{\sigma_n \sum A_i \sin\ \alpha - W\ \tan\ \alpha} \tag{47}$$

where n is the number of faces on the block, i is the index denoting the face of the block, W is the weight of the wedge, A_i is the area of the wedge face, and α is the complement of the joint's dip angle that creates the face. The mechanical properties of the jointed rock masses include an elastic modulus of 32 GPa, Poisson's ratio of 0.25, density of 2000 kg/m^3, joint shear and normal stiffness $K_n = K_s = 10$ MPa/m, and gravity $g = 10$ m/s^2. The analytical critical friction angle is calculated as 34.402°.[25]

The model is first calculated by fixing all the blocks surrounding the wedge and assigning the in-situ stress. Next, beginning from the previous stage, a number of simulations with different friction angles are conducted. The critical angle is numerically obtained from the curve of the final displacement versus the friction angle (see Fig. 13b). The critical angle predicted by the DLSM is 35.5, and the error between the DLSM and analytical solution is only 3.19%. This error could be caused by many factors,

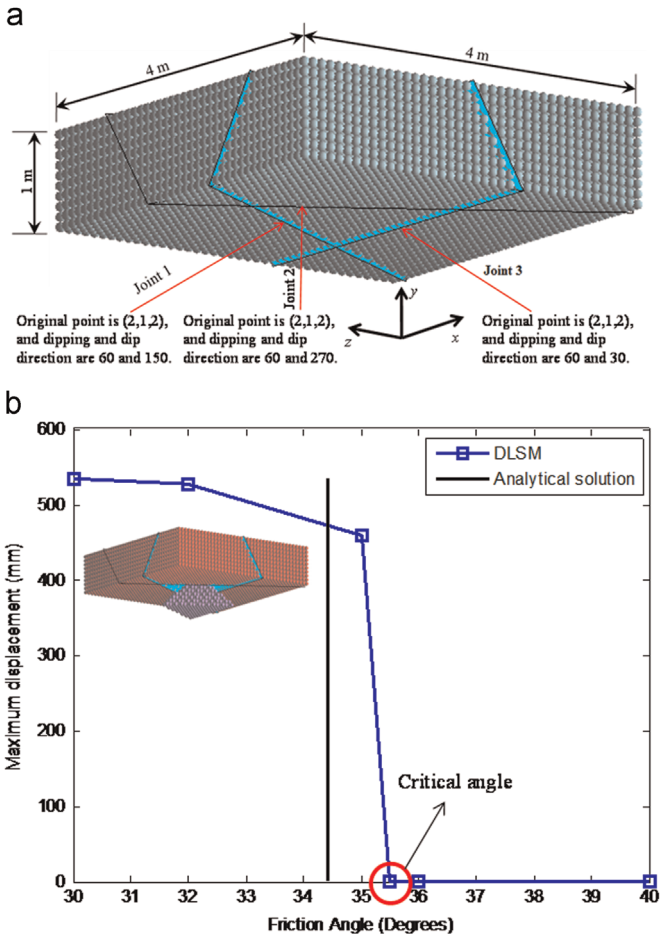

Fig. 13. DLSM simulation of the falling 3D wedge problem.

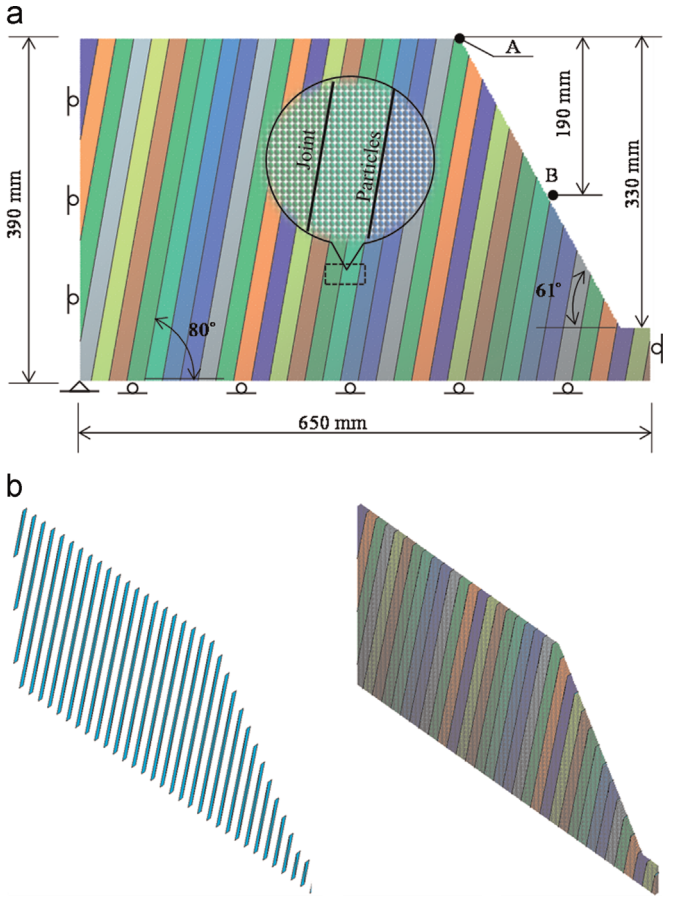

Fig. 14. Computational model built in the DLSM for the jointed slope failure problem.

such as the rigid assumption in the analytical solution being approximated in the DLSM (the rock block is deformable in the DLSM), the spatial representation of the jointed rock masses by a group of particles, etc. Even so, the error is still acceptable for rock engineering purposes. This example indicates that the DLSM can be a useful tool in the stability analysis of jointed rock masses.

3.5. Failure of a jointed slope

The fracturing of jointed rock masses is a complex problem.[28] In this section, the improved DLSM is used to tackle a classical problem concerning the fracturing of jointed rock masses. A number of centrifugal tests on the failure of jointed slopes have been carried out in[29] and later simulated using both the FEM[11] and the DEM.[30] Therefore, this topic is an appropriate example with which to test the DLSM and compare the results with the experimental and numerical results obtained from different methods. The computational model for the DLSM is shown in Fig. 14. Its height is 390 mm, its width is 650 mm, the slope height is 330 mm, and the slope dip angle is 61°. A set of joints with dip angles of 80 and joint spacing of 10 mm is placed in the model. Two detection points (A and B) are also placed in the slope model to record the horizontal displacement history, which was also recorded during the centrifugal test.[28] The material parameters of the block are taken from,[30] including an elastic modulus of 2.4 GPa, Poisson's ratio of 0.16, and density of 2380 kg/m^3. The mechanical parameters of the joints include normal and shear stiffnesses of 400 GPa/m, friction angle of 24°, tensile strength of 0 kPa, and cohesion of 5 kPa. A simple elasto-brittle constitutive model is used for the block. Only normal spring failure is considered, and a single failure parameter u_n^* is required. The experimental data on the horizontal displacement of detection points A and B are used to calibrate this parameter, which significantly influences the history curves of detection points A and B produced by the DLSM. After a trial and error process, the calibrated value of u_n^* is 1.8e−4 mm. The simulated and experimental curves are shown in Fig. 15a. It is concluded that the DLSM can produce similar displacement curves to those observed in the experimental test and produced by the FEM[11] and DEM.[30] In fact, the results given by the DLSM fit more local details over the experimental curves than those generated by the FEM[11] and DEM[30] for a reason explained below. To create a comprehensive comparison, the failure patterns of the experimental approximation and numerical results produced by the DEM,[30] FEM[11] and DLSM are plotted together in Fig. 15b, which shows that the DLSM produces the best fit with the experimental observation. However, the author is hesitant to declare that the DLSM is superior to the FEM[11] and DEM[30] when modelling this problem due to the small particle size (2 mm) adopted in the DLSM simulation. Approximately half a million particles are used for the computational model, which is solved using the parallel DLSM[31] and takes the advantage of the DLSM on high performance computing. It is safe to conclude that the DLSM shows promise at solving problems involving the fracture of jointed rock masses (as an extension of the advantages LSM possesses for jointed rock mass problems).

Difficulty on selection of micro-parameters is the main shortcoming of discontinuum-based models. To overcome this shortcoming, the basic principle adopted in the DLSM is to use parameters that can be easily determined through experiments.

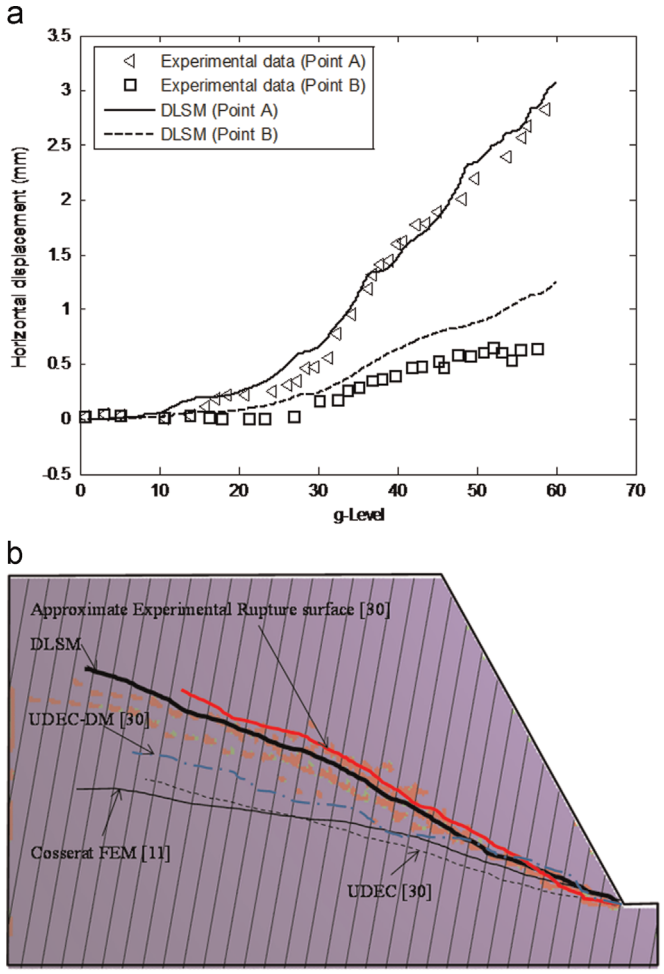

Fig. 15. Displacements and failure patterns predicted by the DLSM.

The corresponding micro-parameters are calculated using closed/empirical equations with these input parameters and the particle model information. For example, a closed relationship between spring stiffness and macroscopic elastic parameters was developed in DLSM.[20] The spring stiffness can directly be determined from the Elastic modulus, the Poisson's ratio, and the lattice coefficient.[20] The joint parameters follow the same principle. The parameters of discontinuum based spring are calculated according to the input joint parameters and the representative area obtained by using Eq. (23). However, as a newly developed method, the DLSM is not perfect and will require further improvement. For example, the DLSM is still unsuitable for solving large deformation problems involving jointed rock masses due to the fact that new contacts between joints under very large deformation are not considered in the current version. This issue will be considered in future work.

4. Conclusion

This work further develops the DLSM for jointed rock masses. The basic concept involves representing jointed rock masses with a group of particles linked by spring bonds. Continuum-based spring bonds are used to model rock blocks, whereas joints are modelled using discontinuum-based spring bonds. The joints are geometrically represented by a group of triangles, and the discontinuum-based spring bonds are formed from a cutting operation between the continuum-based spring bonds and the triangles. Constitutive models, the elasto-brittle model and the Mohr–Coulomb model are also developed for the continuum- and discontinuum-based spring bonds. These techniques can be easily implemented into the DLSM. Using several numerical examples, the study demonstrates that the improved DLSM can successfully solve problems involving jointed rock masses.

Acknowledgement

This research was financially supported by the Australian Research Council (Grant no. DE130100457).

References

1 Goodman RE, Taylor RL, Brekke TL. A model for the mechanics of jointed rock. *J Soil Mech Found Div ASCE.* 1968;94(SM3)637–659.
2 Belytschko T, Moes N, Usui S, et al. Arbitrary discontinuities in finite elements. *Int J Numer Methods Eng.* 2001;50(4)993–1013.
3 Cundall PA. A computer model for simulating progressive large scale movements in blocky rock systems. In: *Proceedings of the International Symposium on Rock Fracture*, Nancy. October, International Society for Rock Mechanics (ISRM), 1, Paper no. II–8; 1971:129–136.
4 Shi GH, Goodman RE. Two dimensional discontinuous deformation analysis. *Int J Numer Anal Methods Geomech.* 1985;9(6)541–556.
5 Zhang X, Lu M, Wegner JL. A 2-D meshless model for jointed rock structures. *Int J Numer Methods Eng.* 2000;47:1649–1661.
6 Yvonnet J, Ryckelynck D, Lorong P, et al. A new extension of the natural element method for non-convex and discontinuous problems: the constrained natural elememt method (C-NEM). *Int J Numer Methods Eng.* 2004;60(8)1451–1474.
7 Wang J, Wu H, Gu CS, et al. Simulating frictional contact in smoothed particle hydrodynamics. *Sci China Technol Sci.* 2013;56(7)1779–1789.
8 Crotty JM, Wardle LJ. Boundary integral analysis of piecewise homogeneous media with structural discontinuities. *Int J Rock Mech Min Sci.* 1985;22(6)419–427.
9 Jing L. A review of techniques, advances and outstanding issues in numericalmodelling for rock mechanics and rock engineering. *Int J Rock Mech Min Sci.* 2003;40:283–353.
10 Swoboda G, Shen XP, Rosas L. Damage model for jointed rock mass and its application to tunnelling. *Comput Geotech.* 1998;22(3–4)183–203.
11 Adhikary DP, Guo H. An orthotropic Cosserat elasto-plastic model for layered rocks. *Rock Mech Rock Eng.* 2002;35(3)161–170.
12 Jia P, Tang CA. Numerical study on failure mechanism of tunnel in jointed rock mass. *Tunn. Undergr. Space Technol..* 2008;23(5)500–507.
13 Ivars DM, Pierce ME, Darcel C, et al. The synthetic rock mass approach for jointed rock mass modelling. *Int J Rock Mech Min Sci.* 2011;48(2)219–244.
14 Tang CA, Zhang YB, Liang ZZ, et al. Fracture spacing in layered materials and pattern transition from parallel to polygonal fracture. *Phys Rev E.* 2006;73(5–2)1–9 056120.
15 Beer G. An isoparametric joint/interface element for finite element analysis. *Int J Numer Methods Eng.* 1985;25:585–600.
16 Osher S, Sethian JA. Fronts propagating with curvature dependent speed: algorithms based on hamilton–jacobi formulations. *J Comput Phys.* 1988;79:12–49.
17 Munjiza A, Andrews KRF. Penalty function method for in combined finite-discrete element systems comprising large number of separate. *Int J Numer Methods Eng.* 2000;49:1377–1396.
18 Simo JC, Laursen TA. An uugmented Lagrangian treatment of contact problems involving friction. *Comput Struct.* 1992;42:97–116.
19 Zheng H, Jiang W. Discontinuous deformation analysis based on complementary theory. *Sci China Ser E Technol Sci.* 2009;52(9)2547–2554.
20 Zhao GF, Fang J, Zhao J. A 3D distinct lattice spring model for elasticity and dynamic failure. *Int J Numer Anal Methods Geomech.* 2011;35:859–885.
21 Zhao GF, Zhao J. Discontinuum based micromechanics methods. In: *Proceedings of the International Conference on Analysis Discontinuous Deformation* (ICADD10); 2012:55 66.
22 Zhao GF, Fang JN, Zhao J. A MLS-based lattice spring model for simulating elasticity of materials. *Int J Comput Meth.* 2012;9(1250037)1–22.
23 Shewchuk JR. Delaunay refinement algorithms for triangular mesh generation. *Comput Geom: Theory Applic.* 2002;22(1–3)21–74.
24 Hoek E, Bray JW. *Rock Slope Engineering.* 2nd ed.,London: Inst Min Metall; 1977.
25 Itasca Inc. *3DEC-3-Dimensional Distinct Element Code, Version 4.10.* Minneapolis: Itasca Consulting Group; 2013.
26 He L, An XM, Ma GW, et al. Development of three-dimensional numerical manifold method for jointed rock slope stability analysis. *Int J Rock Mech Min Sci.* 2013;64:22–35.
27 Goodman RE, Shi GH, Boyle W. Calculations of support for hard, jointed rock using the keyblock principal, issues in rock mechanics. In: *Proceedings of the 23rd Symposium on Rock Mechanics*. University of California Berkeley August, New York, Society of Mining Engineers; 1982:883–898.
28 Jiao YY, Zhang XL, Zhao J. A two-dimensional DDA contact constitutive model for simulating rock fragmentation. *J Eng Mech ASCE.* 2012;138(2)199–209.
29 Adhikary DP, Dyskin AV, Jewell RJ, et al. A study of the mechanism of flexural

toppling failure of rock slopes. *Rock Mech Rock Eng.* 1997;30:75–93.
30 Alzoubi AK, Martin CD, Cruden DM. Influence of tensile strength on toppling failure in centrifuge tests. *Int J Rock Mech Min Sci.* 2010;47:974–982.
31 Zhao GF, Fang JN, Sun L, et al. Parallelization of the distinct lattice spring model. *Int J Numer Anal Meth Geomech.* 2013;37(1)51–74.
32 You S, Zhao GF, Ji HG. Model for transversely isotropic materials based on Distinct Lattice Spring Model (DLSM). *J Comput.* 2012;6(6)1139–1144.